Optofluidic Fano resonance photonic crystal refractometric sensors

Shuling Wang, Yonghao Liu, Deyin Zhao, Hongjun Yang, Weidong Zhou, and Yuze Sun

Citation: Appl. Phys. Lett. **110**, 091105 (2017); doi: 10.1063/1.4977563
View online: http://dx.doi.org/10.1063/1.4977563
View Table of Contents: http://aip.scitation.org/toc/apl/110/9
Published by the American Institute of Physics

Optofluidic Fano resonance photonic crystal refractometric sensors

Shuling Wang, Yonghao Liu, Deyin Zhao, Hongjun Yang, Weidong Zhou,[a] and Yuze Sun[b]
Department of Electrical Engineering, University of Texas at Arlington, Arlington, Texas 76019, USA

(Received 18 December 2016; accepted 14 February 2017; published online 28 February 2017)

We report an ultra-compact surface-normal optofluidic refractometric sensor based on a two-dimensional silicon photonic crystal on insulator. In contrast to the conventional symmetric Lorentzian resonance that is prevalently used in the label-free sensors, the asymmetric lineshape and steep peak-to-dip transition of a Fano resonance enable the enhanced detection sensitivity. The detection limit of 1.3×10^{-6} refractive index units is achieved, which is among the lowest reported experimentally in the defect-free photonic crystal sensors. *Published by AIP Publishing.*
[http://dx.doi.org/10.1063/1.4977563]

A variety of optical structures are being explored for developing highly sensitive, compact, and multiplexed label-free sensor arrays in applications ranging from point-of-care biomedical diagnostics to homeland security,[1–3] including surface plasmon resonance (SPR),[4] metallic nanohole-array-based plasmonics,[5] ring resonators,[6] and one-dimensional (1D) and two-dimensional (2D) photonic crystals.[7–15] Owing to the unique light confinement and enhanced light-matter interaction at the sub-micrometer to nanometer scale, photonic crystal based technology holds great promise for building the ultra-compact and highly sensitive integrated sensor arrays on-chip.

One of the most extensively studied photonic crystal label-free sensors is those with defect cavities and waveguides with in-plane light coupling.[7,9,10,13,14] In order to achieve better sensing performance, i.e., lower detection limit (DL), both high quality factor (Q-factor) and high sensitivity are preferred.[16] Unfortunately, most of the photonic crystal sensors demonstrated to date have either high Q-factor or high sensitivity, but not both. Although slotted photonic crystal waveguide[14] has been promising to achieve both high-Q and high sensitivity, analytes have to be present in the narrow slot region (~200 nm). Therefore, the detection speed greatly comprises due to the slow mass transport rate for the analytes to diffuse in and out of the confined nanoscale channels.

Another major drawback of photonic crystal defect cavities and waveguides is that they require delicate alignment in order to couple the light from free space to in-plane waveguide, making such devices unsuitable for device miniaturization and hence scale-up into multiplexed sensor arrays on chip and for applications in the point-of-care sensing. On the contrary, guided resonances in the defect-free photonic crystal can be conveniently excited using a surface-normal characterization setup through the phase-matching of the out-of-the-plane radiation modes and the in-plane guided modes.[17,18] Such surface-normal configuration greatly relaxes the alignment constraints for light coupling from/to the photonic crystal sensors. The excitation of photonic crystal sensor arrays at normal incidence is also feasible for developing a high-throughput multiplexed label-free biomolecular screening system on chip. Additionally, the defect-free photonic crystal has relatively simple fabrication processes and greater tolerance to the fabrication imperfections in the periodic lattice structures.

The guided resonance in the 2D photonic crystal exhibits Fano resonance shape.[17,19] Unlike the conventional symmetric Lorentzian resonance, the Fano resonance has an asymmetric lineshape that leads to a sharp peak-to-dip transition in the resonance profile and therefore exhibits a higher Q-factor in comparison with its Lorentzian counterpart. Taking advantage of the sharp transition region of the asymmetric Fano lineshape in the reflection or transmission spectrum, a small spectral shift induced by refractive index (RI) change near the photonic crystal region can be extracted and thus better DL can be achieved. To date, although theoretical studies show that DL of 10^{-6}–10^{-7} RIU (refractive index units) can be realized with 2D photonic crystal,[20,21] no experimental work has actually been carried out beyond 10^{-3} RIU.[8,11,21] The actual DL under more realistic conditions remains elusive.

In this paper, we demonstrate the Fano resonance 2D photonic crystal based miniature label-free refractometric sensors that have a high Q-factor and a high sensitivity. We report the design, fabrication, characterization, and analysis of this integrated optofluidic RI sensor. RI sensing with small RI change (10^{-4}–10^{-5} RIU) is systematically studied. A change of 2.8×10^{-5} RIU in bulk liquid is measured experimentally. An extrapolated DL of 1.3×10^{-6} RIU is demonstrated, which is among the lowest reported experimentally in the defect-free photonic crystal sensors.

Fig. 1(a) shows the schematic of 2D photonic crystal that consists of a square lattice of air holes on a silicon-on-insulator (SOI) substrate. Fundamentally, the sensitivity of an RI sensor is determined by the strength of light-matter interaction, which is proportional to the fraction of light present in the bulk solution near the sensor surface.[22] The DL is inversely proportional to the Q-factor of the photonic crystal resonance, as explained later. To search for a high Q and high sensitivity design for liquid sensing, we perform simulation and optimize the device geometry that includes slab thickness (t), lattice constant (a), and air hole radius (r), as illustrated in Fig. 1(b). The reflection spectrum of a Fano resonance is computed based on the Fourier Modal Method

[a]wzhou@uta.edu
[b]sun@uta.edu

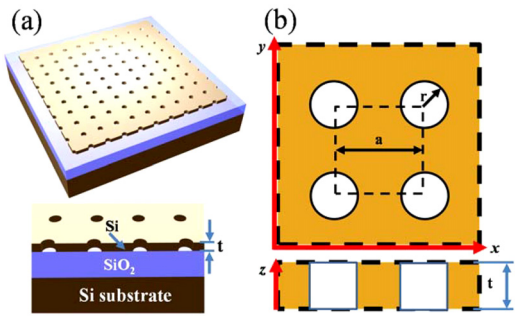

FIG. 1. (a) Schematic of 2D Si photonic crystal on SOI substrate: device overview (top) and cross-sectional view (bottom). (b) Illustration of photonic crystal design parameters: slab thickness (t), lattice constant (a), and air hole radius (r).

using the Stanford Stratified Structure Solver (S^4) software package.[23] The modal field is then calculated based on the finite-difference time-domain (FDTD) method using MEEP,[24] in which the unit cell is defined with the periodic boundary conditions in the xz and yz planes and perfectly matched layers on the top and bottom. A plane continuous-wave source is launched from the top of photonic crystal to excite the Fano resonance mode. With $t = 160$ nm and $r = 0.1a$, the photonic crystal sensor has a Q-factor of 10 000. Sensitivity as high as 300 nm/RIU in the aqueous medium can be achieved. These parameters are subsequently used in our device fabrication.

To fabricate the photonic crystal sensor, the top Si layer thickness of an SOI wafer is first reduced from 260 nm to about 160 nm by thermal oxidation and hydrofluoric acid wet etching. The photonic crystal is fabricated with electron-beam lithography and reactive-ion etching processes, as detailed in our previous work.[25] The scanning electron microscope (SEM) characterization shows that the fabricated photonic crystal sensor has a lattice constant of 970 nm, air hole radius of 103 nm, and slab thickness of 156 nm, as shown in Fig. 2. The fabrication process is simple and compatible with the existing MEMS fabrication technologies. Therefore, mass-production and scale-up to an array format for multiplexed detection are possible with low cost. The schematic of the optofluidic photonic crystal refractometric sensors is shown in Fig. 3(a). The individual photonic crystal patterned area has a dimension of $500 \times 500\,\mu m^2$. According to the simulation results, the size of the device can be further decreased to $40 \times 40\,\mu m^2$ without compromising the Q-factor or bulk RI sensitivity. A polydimethylsiloxane (PDMS) microfluidic flow cell is fabricated using soft lithography and then bonded to the photonic crystal device for sample delivery.

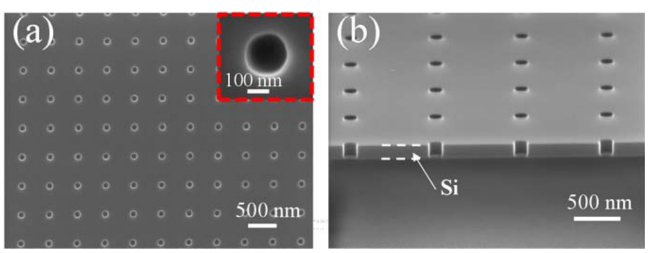

FIG. 2. SEM images of the fabricated photonic crystal on SOI substrate. (a) Top view showing the lattice constant $a = 970$ nm and air hole radius $r = 103$ nm. Inset shows the zoomed-in image of the air hole. (b) Cross-sectional view showing the Si slab thickness $t = 156$ nm.

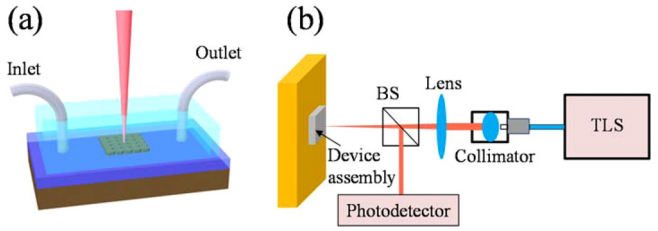

FIG. 3. (a) Schematic of photonic crystal optofluidic refractometric sensors (not to scale). The photonic crystal ($500 \times 500\,\mu m^2$) is enclosed in a PDMS flow cell of 35 nL. (b) Schematic illustration of optical characterization setup. A laser beam from the tunable laser source (TLS) is collimated and then focused to the photonic crystal slab surface at normal incidence. The reflection spectrum is measured in real-time by a photodetector.

The experimental setup for device characterization and sensing measurement is illustrated in Fig. 3(b). Light from a tunable laser source (Agilent 81980 A, 1 pm spectral resolution) is collimated and focused onto the photonic crystal at normal incidence. The reflected beam intensity is measured by a photodetector (Agilent 81623B, 100 pW noise level). The experimental setup is controlled by the LabView codes developed in house. The tunable laser is repeatedly scanned in a narrow spectral range covering one Fano resonance mode at 2 Hz, and the reflection spectrum is monitored and recorded in real-time for further analysis. The experimental setup is built on air table to reduce the noise and vibration from the environment.

Fig. 4(a) shows the measured reflection spectrum of the photonic crystal when the microfluidic channel is filled with deionized (DI) water (RI = 1.33). We observe strong resonances at normal incidence, associated with the Fano coupling between free space and guided resonances. The resonance spectral position $\lambda_0 = 1537.5$ nm and a Q-factor of 2,828 are obtained from the Fano fitting.[26] The thickness of the PDMS layer that is interacting with the incident light beam is around 1 mm. The optical loss introduced by the PDMS flow cell is negligible for the Fano resonance mode (loss coefficient $\alpha_{1550\,nm} = 0.67$ dB/cm[27]). To characterize device bulk liquid RI sensitivity, various concentrations of ethanol/DI water mixture (0.05%–0.3%, v/v) with known RI are flowed into the microfluidic channel using a syringe pump at a flow rate of 0.1 ml/min. DI water rinsing is carried out between two consecutive sample measurements to ensure that the microfluidic channel is free of residual ethanol. The spectral shift ($\Delta\lambda$) is read out from the linear region of the peak-to-dip transition in a Fano resonance. Specifically, linear fitting is performed in the peak-to-dip transition region of a Fano resonance mode. The intensity change (ΔI) is monitored in real-time at the point where $I = (I_{peak} + I_{dip})/2$ of the normalized reflection spectrum and then converted into $\Delta\lambda$, which is used as the sensing signal. The corresponding sensorgram for a series of ethanol/DI water samples is presented in Fig. 4(b), from which it clearly shows that Fano resonance spectral position redshifts when ethanol/DI water sample (i.e., RI increase) reaches the sensor surface and returns to signal baseline after DI water rinsing. The respective spectral shift ($\Delta\lambda$) in Fig. 4(b) with RI change (Δn) is plotted out in Fig. 4(c). The linear fitting of the experimental data demonstrates a bulk RI sensitivity of 264 nm/RIU. To compare the

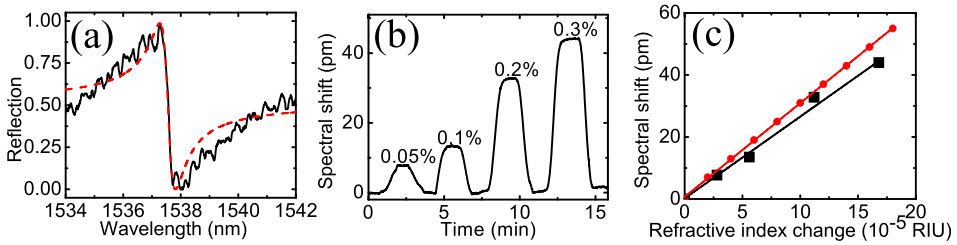

FIG. 4. (a) Experimental (black) and fitted (red) normalized reflection Fano resonance spectra of the photonic crystal in water environment. The spectral position is at 1537.5 nm and the resonance has a Q-factor of 2,828. (b) Sensorgram of Fano resonance spectral response to various concentrations of ethanol-water solution. (c) Fano resonance spectral shift in response to refractive index change: simulation (red) and experimental (black) bulk RI sensitivity.

experimental measurement with the simulation data, the device sensitivity is calculated using S^4 by tracking the shift of the resonance spectral position in the reflection spectrum in regard to the RI increase, as shown in Fig. 4(c). The simulation result shows that the sensitivity is 303 nm/RIU, which is very close to the measurement results. The discrepancy between simulation and measurement may be due to the imperfect shape of air holes from fabrication etching process and slight inaccuracy in the Si slab thickness characterization. The smallest RI change measured in experiment is 2.8×10^{-5} RIU with 0.05% ethanol, which results in a spectral shift of 7.7 pm, well above the 3σ noise ($\sigma = 0.117$ pm). This result represents two orders of magnitude improvement in the bulk liquid RI sensitivity that is actually measured in experiment compared to other photonic crystal based RI sensors reported to date.

To better understand the sensing capability of the photonic crystal sensor, theoretical simulation is performed using the photonic crystal geometry parameters obtained from SEM characterization on the fabricated device. The simulated normalized Fano resonance reflection spectrum is shown in Fig. 5(a), when the device is in water environment. The simulation predicts that the photonic crystal possesses a Fano resonance at $\lambda_0 = 1534.9$ nm with a Q-factor of 5,429.

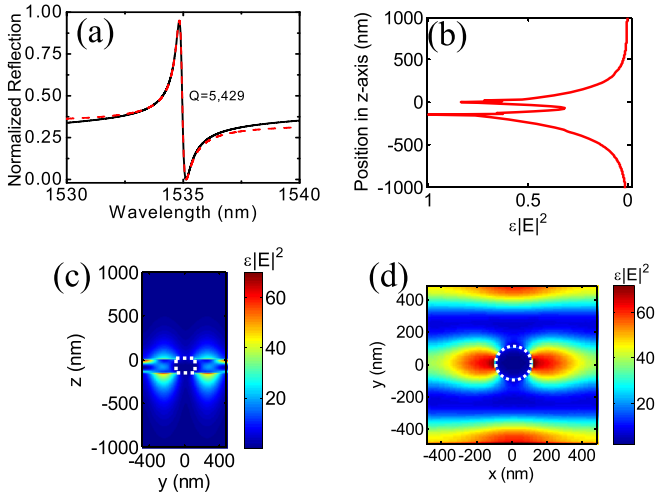

FIG. 5. Simulation of Fano resonance reflection spectrum and electric field distribution when photonic crystal ($t = 156$ nm, $a = 970$ nm, and $r = 103$ nm) top surface is covered with DI water. (a) Calculated (black) and fitted (red) Fano resonance reflection spectrum. The spectral position is at 1534.9 nm, and the resonance has a Q-factor of 5,429. (b) The electric filed energy along vertical direction (z-axis). The sensor surface is located at $z = 0$. (c) and (d) show the mode profile in the yz plane ($x = 0$) and xy plane ($z = 0$), respectively. Dashed lines outline the boundary of the air hole.

The measured Fano resonance spectral position agrees well with the simulated result. The Q-factor obtained in experiment is lower than the simulation prediction, which is attributed mainly to imperfections in fabrication and device surface roughness. Deviation from perfectly shaped circular air holes and non-uniform Si surface can severely lower the Q-factor in experiment. Electric field distribution of the Fano resonance mode used in the sensing experiment is also calculated in Fig. 5. The mode electric field energy ($\varepsilon|E|^2$) distributions in the yz plane in Fig. 5(c) (cross-sectional view) and the xy plane (top view) in Fig. 5(d) reveal that the modal field is localized mainly in the Si slab region and decay evanescently into surrounding low index medium. The sensing principle of photonic crystal sensor is the detection of resonance spectral shift induced from RI change in the surrounding liquid (i.e., near sensor top surface). Using the perturbation theory, the bulk RI sensitivity, S [nm/RIU], is given by[22]

$$S = \frac{\Delta\lambda}{\Delta n} = f\frac{\lambda_0}{n_{liquid}}, \tag{1}$$

where λ_0 is the resonance wavelength, n_{liquid} is the liquid RI, and f is the filling fraction quantifying the relative overlap between the Fano resonance mode and the liquid. To quantitatively evaluate the percentage of light interacting with the liquid near the photonic crystal top surface and in the air holes, the filling fraction is calculated using FDTD. The result shows that 25.9% of the Fano resonance mode is present in the liquid above the sensor top surface and only 0.13% of the mode is present in the air holes of the slab. Therefore, the spectral shift is almost exclusively caused by the RI change in the liquid on the slab surface. According to Eq. (1), the bulk RI sensitivity is 298 nm/RIU, which agrees well with the calculated S by tracking the spectral shift in S^4 and the measured result demonstrated in experiment. In addition, the DL of photonic crystal sensor can be estimated by[16]

$$DL = \frac{R}{S}, \tag{2}$$

where R is the spectral resolution determined by the resonance mode Q-factor (i.e., spectral linewidth) and the noise of the measurement system. In contrast to the conventional symmetric Lorentzian lineshape sensors, our photonic crystal sensor demonstrates an asymmetric Fano lineshape with a sharp peak-to-dip transition, making it advantageous for achieving better DL in practice. To determine the DL of photonic crystal sensor, a representative baseline signal is acquired for 5 min. The standard deviation (σ) of the baseline

signal is measured to be 0.117 pm. Extrapolating to the 3σ threshold, our photonic crystal sensor DL is determined to be $\sim 1.3 \times 10^{-6}$ RIU according to Eq. (2).

In summary, we have presented a Fano resonance photonic crystal based optofluidic RI sensor. The defect-free 2D photonic crystal structure reduces fabrication complexity and enables scale-up to an array format for multiplexed detection on chip. The unique light guiding method of Fano resonance in 2D photonic crystal avoids delicate alignment for light coupling and simplifies the measurement setup. Moreover, the asymmetric lineshape of Fano resonance improves the DL in practice, and a record-low DL of 1.3×10^{-6} RIU is achieved in experiment. Our results lay a foundation for high-precision miniature label-free sensor in biological and chemical analysis.

This work was supported by U.S. NSF 1407947 and U.S. ARO W911NF-15-1-0431.

[1]X. Fan and I. M. White, Nat. Photonics **5**, 591 (2011).
[2]X. Fan, I. M. White, S. I. Shopova, H. Zhu, J. D. Suter, and Y. Sun, Anal. Chim. Acta **620**, 8 (2008).
[3]D. E. W. Patabadige, S. Jia, J. Sibbitts, J. Sadeghi, K. Sellens, and C. T. Culbertson, Anal. Chem. **88**, 320 (2016).
[4]J. Homola, S. S. Yee, and G. Gauglitz, Sens. Actuators, B **54**, 3 (1999).
[5]A. A. Yanik, M. Huang, A. Artar, T.-Y. Chang, and H. Altug, Appl. Phys. Lett. **96**, 021101 (2010).
[6]F. Vollmer, D. Braun, A. Libchaber, M. Khoshsima, I. Teraoka, and S. Arnold, Appl. Phys. Lett. **80**, 4057 (2002).
[7]E. Chow, A. Grot, L. W. Mirkarimi, M. Sigalas, and G. Girolami, Opt. Lett. **29**, 1093 (2004).
[8]M. Huang, A. A. Yanik, T.-Y. Chang, and H. Altug, Opt. Express **17**, 24224 (2009).
[9]M. Lee and P. M. Fauchet, Opt. Express **15**, 4530 (2007).
[10]V. Toccafondo, J. García-Rupérez, M. J. Bañuls, A. Griol, J. G. Castelló, S. Peransi-Llopis, and A. Maquieira, Opt. Lett. **35**, 3673 (2010).
[11]O. Levi, M. M. Lee, J. Zhang, V. Lousse, S. R. J. Brueck, S. Fan, and J. S. Harris, Proc. SPIE **6447**, 64470P1 (2007).
[12]P. S. Nunes, N. A. Mortensen, J. P. Kutter, and K. B. Mogensen, Opt. Lett. **33**, 1623 (2008).
[13]W.-C. Lai, S. Chakravarty, Y. Zou, and R. T. Chen, Opt. Lett. **37**, 1208 (2012).
[14]B. Wang, M. A. Dündar, R. Nötzel, F. Karouta, S. He, and R. W. V. D. Heijden, Appl. Phys. Lett. **97**, 151105 (2010).
[15]I. D. Block, N. Ganesh, M. Lu, and B. T. Cunningham, IEEE Sens. J. **8**, 274 (2008).
[16]I. M. White and X. Fan, Opt. Express **16**, 1020 (2008).
[17]S. Fan and J. D. Joannopoulos, Phys. Rev. B **65**, 235112 (2002).
[18]W. Zhou, D. Zhao, Y.-C. Shuai, H. Yang, S. Chuwongin, A. Chadha, J.-H. Seo, K. X. Wang, V. Liu, Z. Ma, and S. Fan, Prog. Quantum Electron. **38**, 1 (2014).
[19]U. Fano, Phys. Rev. **124**, 1866 (1961).
[20]M. El Beheiry, V. Liu, S. Fan, and O. Levi, Opt. Express **18**, 22702 (2010).
[21]C. Nicolaou, W. T. Lau, R. Gad, H. Akhavan, R. Schilling, and O. Levi, Opt. Express **21**, 31698 (2013).
[22]N. A. Mortensen, S. Xiao, and J. Pedersen, Microfluid. Nanofluid. **4**, 117 (2008).
[23]V. Liu and S. Fan, Comput. Phys. Commun. **183**, 2233 (2012).
[24]A. F. Oskooi, D. Roundy, M. Ibanescu, P. Bermel, J. D. Joannopoulos, and S. G. Johnson, Comput. Phys. Commun. **181**, 687 (2010).
[25]Y. Shuai, D. Zhao, Z. Tian, J.-H. Seo, D. V. Plant, Z. Ma, S. Fan, and W. Zhou, Opt. Express **21**, 24582 (2013).
[26]B. Luk'yanchuk, N. I. Zheludev, S. A. Maier, N. J. Halas, P. Nordlander, H. Giessen, and C. T. Chong, Nat. Mater. **9**, 707 (2010).
[27]M. Andriot, S. H. Chao, A. Colas, S. Cray, F. de Buyl, J. V. DeGroot, A. Dupont, T. Easton, J. L. Garaud, E. Gerlach, F. Gubbels, M. Jungk, S. Leadley, J. P. Lecomte, B. Lenoble, R. Meeks, A. Mountney, G. Shearer, S. Stassen, C. Stevens, X. Thomas, and A. T. Wolf, in *Inorganic Polymers*, edited by R. De Jaeger and M. Gleria (Nova Science Publishers, New York, 2007), p. 61.